Desalination and Water Treatment
www.deswater.com

doi: 10.5004/dwt.2019.23969

153 (2019) 338–348
June

Electrochemical regeneration of granular activated carbon saturated with acid red 18 using a novel modified Ti/Co-MnO_2 electrode

Jalal Basiri Parsa*, Ghazal Meysami, Farnaz Jafari

Applied Chemistry Department, Faculty of Chemistry, Bu-Ali Sina University, Hamedan 65174, Iran, Tel. +98 813 8282808, Fax +98 813 8257407, email: parssa@basu.ac.ir (J.B. Parsa), ghazal.meysami@gmail.com (G. Meysami), f.jafari1991@yahoo.com (F. Jafari)

Received 12 September 2018; Accepted 17 February 2019

ABSTRACT

In this work, the electrochemical (EC) regeneration of granular activated carbon (GAC) saturated with Acid Red 18 (AR18) was investigated using a novel non-active anode of modified Co-MnO_2 in a batch reactor. The study's main objective is the process modelling and optimising using the response surface methodology (RSM) based on a central composite design (CCD). The effective regeneration efficiency (RE) variables included: current density, electrolyte concentration and pH. The optimum values of current density, 0.18 $A \cdot cm^{-2}$, electrolyte concentration, 0.22 $mol \cdot L^{-1}$, and pH, 2.35, were achieved. Additionally, under optimum conditions, a maximum RE of 88% was obtained. After three sequential adsorption–regeneration cycles, only 23 declination was observed in %RE, which confirmed the reuse feasibility of the regenerated GAC. The proposed model's fitness was checked by the determination coefficient ($R^2 = 0.9914$), which demonstrated the agreement between the quadratic model and the experimental results. Additionally, the energy consumption in the EC regeneration of saturated GAC under optimum conditions was calculated as 1.5 ($kW \cdot h \cdot kg^{-1}$).

Keywords: Acid Red 18; Electrochemical regeneration; Granular activated carbon; Central composite design (CCD); Batch reactor

1. Introduction

Azo dyes are synthetic organic compounds that are commonly present in the effluents of many industries, such as textile, leather, food processing, dyeing, cosmetics, paper, etc. These types of dyes are not only aesthetically displeasing but also limit light penetration into rivers and, consequently, the photosynthesis processes are reduced [1]. These compounds resist biological treatment due to the large amount of aromatics in their structure [2].

AR18, a mono-azo toxic dye, causes severe environmental problems due to its high toxicity and carcinogenic effects [3]. Consequently, it is essential to treat these coloured effluents before their final disposal [4] and various methods have been employed to remove dyes from wastewater, including adsorption, coagulation, advanced oxidation and membrane separation [5]. Among the above-mentioned methods, adsorption has become one of the most attractive and effective alternative treatments for dye removal from wastewater because of its high efficiency and low-cost and eco-friendly operations [4,6].

GAC is the most widely-used adsorbent, being highly successful because of its large, porous surface area [7], high adsorption capacity [8], fast adsorption kinetics and ease of regeneration [9]. During the use of GAC, its surface becomes saturated and inactive. It is usually taken to landfill and discarded, which has an economic cost and causes environmental problems [8]. Therefore, regeneration of the exhausted GAC, as the most economical method and environmentally acceptable option, would be suggested [10, 11]. There are various techniques used to regenerate GAC, including microbial [12], microwave [13], thermal [14], chemical [15], electrochemical [16], supercritical fluid (SCF) [17], ultrasound [11], the Fenton mechanism [18] etc. The most widely-used regeneration process in industry is thermal regeneration. However, this technique has serious disadvantages, such as carbon loss and high energy consumption, so it cannot be considered to be an effective method [19].

*Corresponding author.

EC regeneration techniques are very promising alternatives and present several advantages compared to the conventional methods [20], such as, in situ operation without damaging the carbon's structural properties and characteristics, no addition of chemicals [21], low energy consumption [22], short time requirements [8] and high regeneration efficiency [23]. The first investigation into EC regeneration of activated carbon (AC) was performed by Owen and Barry [24], who achieved regeneration efficiencies of up to 61% and introduced EC regeneration as a promising technique. Subsequently, in 1994, Narbaitz and Cen [25] utilised the EC method for the regeneration of AC loaded with phenol. They revealed that EC regeneration achieved high efficiencies without apparent loss of carbon mass and that the RE obtained was around 95%. A 90% RE of AC loaded with p-nitrophenol using a fluidized cylindrical EC reaction for 1.5 h was reported by Zhou and Lei [26]. In this study, the energy consumption per unit kilogram of AC treated was calculated and presented as 2.78 kWh/kg. The performance of the EC regeneration process is strongly dependent on the electrode material, which is fundamentally divided into two main types, an active electrode (such as Pt) and a non-active electrode (such as PbO_2) [27]. In both cases, the oxidation of water molecules is the first reaction occurring in the direct oxidation process, which leads to the formation of hydroxyl radicals (OH) adsorbed on the anode surface. In non-active electrodes, due to the weak interaction with the electrode surface, OH have more opportunities to play their role in the degradation of pollutants, thus achieving better results. On the other hand, for *active electrodes*, direct oxidation occurs through the formation of a higher oxide MO_{x+1} (M is the anode electrode) in the lattice rather than OH, owing to the higher adsorption enthalpy of the MOH [28]. Therefore, electrode modification, to enhance the performance and cost-effectiveness of the regeneration process, has gained greater attention in recent years. Table 1 depicts recent illustrative studies related to EC regeneration using non-modified and modified electrodes, with discussion about operational conditions and reported regeneration efficiencies. However, although the performance of regeneration processes with different modified electrodes was investigated, using modified Ti/Co-MnO_2 electrodes in EC regeneration has not yet been reported. The present study's main objective is to investigate the applicability of EC regeneration of saturated GAC with AR18 in a batch reactor, in the presence of NaCl electrolyte, using a novel modified Ti/Co-MnO_2 electrode prepared using the thermal decomposition technique. Some advantages of this modified electrode include ease of production, cost effectiveness, oxygen evolution catalytically and mechanical stability. The EC regeneration process of the GAC loaded with AR18 was modelled and optimised using the RSM based on the CCD.

2. Experimental

2.1. Chemicals

AR18, an anionic azo dyes with a chemical formula of, a molecular weight of 604.5 g·mol^{-1} and λ_{max} of 506 nm [34], was selected as a model of contaminant and supplied by Alvan Sabet Co., Hamadan, Iran. The dye's chemical structure and its ultraviolet-visible (UV–Vis) spectrum are given in Fig. 1 [35] and Fig. 2 respectively. The dye stock solution was prepared by dissolving an accurate weight of dye in double-distilled water.

The GAC used in this work was purchased from Shimi co., Hamedan, Iran and prepared from walnut shells. The

Table 1
Comparison of electrochemical regeneration of GAC using non-modified and modified electrodes

Electrolyte	Non-modified electrode						
	Current density (A/cm^2)	Range of time (h)	Cathode	Anode	Contaminate	RE%	Ref.
NaCl	0.001	5	Platinum	Platinum	Phenol	80	[29]
NaCl	0.001	2.5	Platinum	Platinum	Organic matter	80	[23]
NaCl	0.008	12	Graphite	Graphite	Leachate	91.1	[26]
NaCl	0.002	5	Platinum	Platinum	Organic compounds	20	[30]
Na_2SO_4	0.003	1.5	Titanium mesh	Titanium mesh	Rhodamine B	83.7	[31]
	Modified electrode						
Electrolyte	Current density (A/cm^2)	Range of time (h)	Cathode	Anode	Contaminate	RE%	Ref.
NaCl	0.002	0.16	Stainless Steel	Iridium-based mixed metal oxide coated titanium	Crystal violet dye	95	[10]
NaCl	0.006	1.5	Stainless Steel	β-PbO_2	*p*-nitrophenol	90	[32]
Na_2SO_4	0.02	2.5	Stainless Steel	SnO_2/Ti	Organic compounds	100	[21]
NaOH	0.05	3	Stainless Steel	SnO_2-Sb/Pt	Phenol	84	[20]
NaOH	0.05	3	Stainless Steel	Platinized titanium (Pt/Ti)	Phenol	80	[8]
NaCl	0.29	2	platinized titanium(Pt/Ti)	Platinized titanium(Pt/Ti)	Phenol	100	[33]

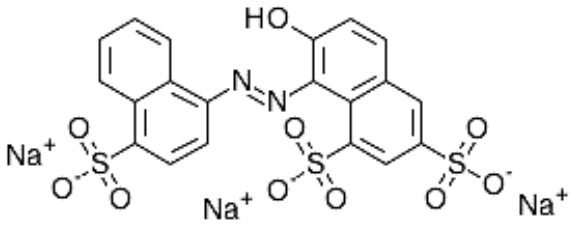

Fig. 1. The structure of AR18 [30].

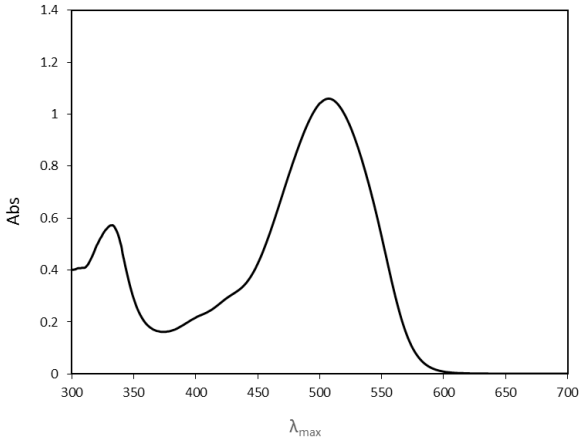

Fig. 2. UV–visible spectrum of AR18.

adsorbent was sieved through sieves no. 10 and 16 to obtain GAC grains between 1.19 mm and 2 mm in diameter. It was then washed several times with hot deionised water to eliminate surface impurities and was dried in an oven for 6 h to constant weight at 100°C.

In this study, all the chemicals were used without further purification. Sulfuric acid (0.1 M) and sodium hydroxide (0.1 M) were used for the pH adjustment and were purchased from Merck. Deionised water was used in all the experiments.

2.2. Method

2.2.1. Adsorption isotherm of AR18

The adsorption experiments were carried out using a batch setup, to determine the concentration required to achieve the equilibrium and adsorption capacity of GAC. A specific amount of GAC (0.3 g) was put into the flasks with equal volumes (200 mL) and different initial concentrations of AR18 (200–2000 mg·L^{-1}) and stirred on a magnetic mixer for 24 h until equilibrium was established. The remaining dye concentration was determined using a UV/Vis spectrophotometer (Jasco-V630) at the maximum wavelength of 506 nm. The amount of dye adsorbed onto the GAC was determined by the mass balance Eq. (1).

$$q = \frac{V\left(C_0 - C_e\right)}{M} \tag{1}$$

where q is the amount of AR18 onto GAC (mg·g^{-1}), V is the volume of the solution (L) and M is the weight of GAC. C_0 and C_e are the initial and equilibrium liquid-phase concentration of AR18 (mg·L^{-1}), respectively.

2.2.2. Preparation of the MnO_2/Ti electrodes

The novel electrode consists of a valve metal base, or of a metallic alloy having similar characteristics to those of valve metals, or a base of electrically-conductive material that is corrosion-resistant to the anodic condition having, on at least one part of its outer surface, an electrocatalytic coating of B-type manganese dioxide chemically deposited by means of the thermal decomposition of an alcoholic solution of manganese nitrate. Among the valve metals, such as aluminium, molybdenum and titanium, the preference, based on cost, availability and electrical and chemical properties, is to use titanium. These anodes are also particularly suited for the electrolytic production of perchlorates. The Ti/Co-MnO_2 electrode was prepared using the thermal decomposition technique, which consisted of the following process:

The Ti electrode (20 mm*100 mm*0.5 mm) was etched in boiling 20% HCl solution for 30 min. $Mn(NO_3)_2$ was dissolved in ethanol to prepare a solution with a concentration of 50 g/l. The β-manganese dioxide coating is further catalytically activated by doping with up to 5% by weight of a metal selected from group IB, IIB, IVA, VB, VIB, VIIB, or VII of the periodic table, excluding the platinum metals, gold and silver. Cobalt is the preferred metal owing to the excellent results of coating doped with this metal. The doping metal, such as cobalt, added to the manganese nitrate solution is used in the form of a thermally decomposable salt, such as its nitrate. The etched Ti electrode was soaked in $Mn(NO_3)_2$ 50 g·L^{-1} solution doped with up to 5% by weight of $Co(NO_3)_2$ and then placed in the oven (containing oxygen) at 300°C, after which the thermal decomposition had completely occurred within 10 min [36]. The above soaking and heating processes were repeated 10 times to obtain the desired thickness of the β-MnO_2 coating. The coating electrodes' morphology was examined using scanning electron microscopy (SEM) (JSM/840A).

2.2.3. Apparatus

In this work, the GAC regeneration was carried out in a stirred EC batch reactor. Fig. 3 depicts a schematic diagram of the experimental setup. Graphite and Ti/MnO_2 plates with an active area of 6 cm^2 (2 cm × 3 cm) were used as the cathode and anode electrode, respectively. The electrodes were maintained at a separation distance of 2 cm and submerged in the NaCl electrolyte. A magnetic stirrer (Alfa, HS-860) was used to mix the solutions. The electric current was provided by a DC power supply (APS-1363P).

2.2.4. Electrochemical regeneration

The regeneration procedure was evaluated by using the following procedures:

i. Initial adsorption: This was conducted in a stirred beaker, with 9 g of dried GAC mixed with 600 mL of 10000 mg·L^{-1} AR18 solution and stirred using a magnetic mixer for 24 h at room temperature to achieve equilibrium.

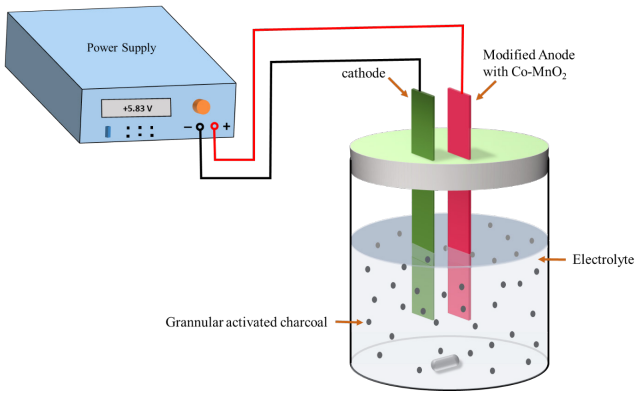

Fig. 3. The schematic diagram of the experimental setup.

ii. EC regeneration: 0.5 g of the exhausted GAC was placed into the EC reactor with 200 mL of NaCl solution to be regenerated. The EC regeneration of GAC began when the direct current power supply was turned on. The current density, the NaCl concentration and the pH parameters are considered as the variables that must be optimised. The solutions' pH was measured using a pH meter (Denver, UB-10). The regeneration time in this study was maintained at a constant time of 1 h.
iii. Re-adsorption: The regenerated GAC samples were used for the re-adsorption of AR18 under the same conditions as the initial adsorption (step i) to indicate RE. For the adsorption/EC regeneration over a number of cycles, steps (ii) and (iii) were repeated.

2.2.5. Experimental design

The experimental design method provides statistical models for process variable optimisation. In this work, the optimum operating conditions, the experimental variables' effects on RE and the interactions between them with a minimum number of experiments were estimated by employing the CCD of RSM. The variables studied in this project included the current density, the electrolyte concentration and the pH. The determination of the optimum set of operational variables of a process is the major target of RSM and it is comprised of three basic steps: (a) experimental design; (b) response surface modelling; and (c) process optimisation [37]. Design-Expert software (version 7, trial) was used to design the experiments and for the experimental data analysis.

2.2.6. Analysis

The adsorption capacity of fresh GAC and the re-adsorption capacity of regenerated GAC were comprised to demonstrate the effectiveness of the regeneration process.

1. The percent regeneration efficiency (%RE) was calculated from Eq. (2):

$$\%RE = \frac{q_r}{q_e} \times 100 \quad (2)$$

where q_r and q_e are the adsorptive capacity of regenerated and fresh GACs, respectively.

2. Measuring the adsorption isotherm of nitrogen at 77 K was performed to complete the investigation of the textural changes of GAC during EC regeneration. The %RE was calculated using Eq. (3) [31]:

$$\%RE = \frac{a_{reg} - a_{sat}}{a_{fresh} - a_{sat}} \times 100 \quad (3)$$

where a_{reg}, a_{sat} and a_{fresh} are the regenerated, saturated and fresh of GAC surface area, respectively.

3. Result and discussion

3.1. Adsorption isotherms

The AR18 adsorption isotherms onto GAC are depicted in Fig. 4. Fresh GAC adsorbed the highest value of the quantity of AR18 (96.59 mg·g^{-1}). The large surface area (840.046 m^2·g) is the main reason for the high adsorption capacity of GAC.

3.2. Experimental design and optimisation

The most popular class of second-order designs, the CCD of the RSM, was used to optimise the effective process variables. The experiment conditions' details were adjusted based on the experimental design matrix, as provided in Table 2.

The total number of experiments (N) was calculated as the sum of the 2^k factorial runs, the 2^k axial runs and the N_0 center runs. ($N = 2^k + 2k + N_0$), where k is the number of factors. Hence, the total number of tests required for the three factors was identified as 20, including 8 factorial points, 6 axial points and 6 replicates at the center point. The center points are used to determine the experimental error and the data's reproducibility. Based on the ranges attained by the preliminary experiments, each of the variables was coded at five different levels between $-\alpha$ and $+\alpha$ ($-\alpha$, -1, 0, $+1$, $+\alpha$). Table 3 shows the experimental range in terms of the coded factors. The regeneration efficiency (%RE) after 60 min was considered as the response.

The response, as a function of variables and their interaction, was predicted using a quadratic polynomial empirical model. The experimental data was fitted to a quadratic model, according to Eq. (4):

$$Y = \beta_0 + \sum_{j=1}^{n} \beta_j X_j + \sum_{j=1}^{n} \beta_{jj} X_j^2 + \sum_i \sum_{<j=2}^{n} \beta_{ij} X_i X_j + e_i \quad (4)$$

where Y is the predicted response, β_0, β_j, β_{jj} and β_{ij} represent the constant term, the linear coefficient, the quadratic coefficient and the interaction coefficient, respectively. X_i and X_j are influencing parameters, n is the number of variables and e_i shows the error.

The analysis of variance (ANOVA) has confirmed the proposed model's significance and adequacy. The interaction between the process variables (A: Current density, B: electrolyte concentration and C: pH) and the response were evaluated by the ANOVA and showed a good agreement for the data with a quadratic model. This quadratic model's ANOVA results are listed in Table 4 [19,38].

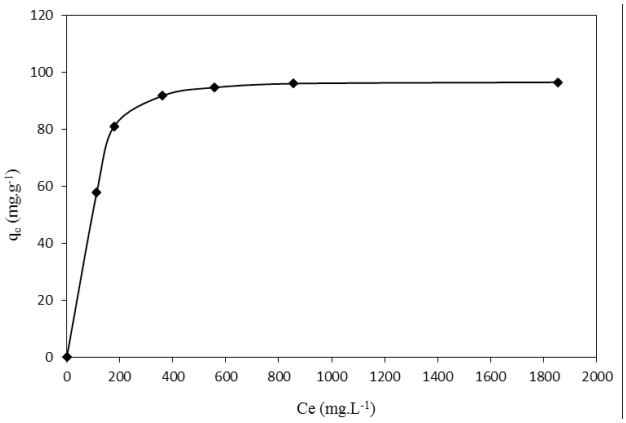

Fig. 4. Adsorption isotherms of AR18 on fresh GAC.

Table 2
The central composite design matrix for three independent variables and observed response

Experimental run	Current density ($A \cdot cm^{-2}$)	Electrolyte concentration ($mol \cdot L^{-1}$)	pH	Regeneration efficiency (%)
1	0.06	0.29	6.78	45
2	0.13	0.05	5.00	53
3	0.13	0.20	5.00	63
4	0.20	0.11	6.78	55
5	0.13	0.35	5.00	62
6	0.13	0.20	5.00	61
7	0.06	0.11	3.22	53
8	0.20	0.29	3.22	84
9	0.13	0.20	2.00	88
10	0.20	0.29	6.78	60
11	0.25	0.20	5.00	58
12	0.13	0.20	5.00	64
13	0.06	0.11	6.78	45
14	0.13	0.20	8.00	60
15	0.01	0.20	5.00	32
16	0.13	0.20	5.00	62
17	0.20	0.11	3.22	68
18	0.13	0.20	5.00	60
19	0.06	0.29	3.22	60
20	0.13	0.20	5.00	59

Table 3
The experimental ranges and levels of variables in terms of real and codded factors

	$-\alpha$	–1	0	+1	$+\alpha$
Current density, X_1 ($A \cdot cm^{-2}$)	0.01	0.06	0.13	0.20	0.25
Electrolyte concentration, X_2 ($mol \cdot L^{-1}$)	0.05	0.11	0.2	0.29	0.35
pH, X_3	2	3.22	5	6.78	8

The correlation between the actual experimental and the predicted data was evaluated by the regression coefficient (R-seq and the value of adj. R-seq) [39]. The value of R^2 and adjusted R^2 is close to 1.0, demonstrating the model's ability in predicting the process behaviour in the design space. The evaluation of the proposed model's predictive ability was carried out by using RMSEP and RSEP. The RMSEP and RSEP were computed as:

$$RMSEP = \sqrt{\frac{\sum_{i=1}^{n}\left(y_{pred,i} - y_{meas,i}\right)^2}{n}} \tag{5}$$

And

$$RSEP = \sqrt{\frac{\sum_{i=1}^{n}\left(y_{pred,i} - y_{meas,i}\right)^2}{\sum_{i=1}^{n}\left(y_{meas,i}\right)^2}} \times 100 \tag{6}$$

where ($y_{pred,i}$)and ($y_{meas,i}$) are the predicted and modelled values of the response (Y) and n represents the number of experiments [40].

From the ANOVA results, the Prob > F and F-value of the second order model attained less than 0.0001 and 127.87, respectively. These mentioned results imply the proposed model's significance. The second-order polynomial model, displaying the empirical relationship between the response and the variables, is given in Eq. (7):

$$\%RE = 61.50 + 7.89A + 3.16B - 7.84C + 1.75AB - 1.75AC - 2.25BC - 5.82A^2 - 1.40B^2 + 4.44C^2 \tag{7}$$

The synergic effect of each term is shown by a positive sign, whereas the antagonistic effect is indicated by a negative sign [19].

Strong agreement was also found between the experimental and the predicted value of %RE, as revealed by the high value of the determination coefficient (R^2 = 0.9914). Additionally, a reasonable agreement with (adjusted R^2 = 0.9836) showed the model's high significance. The proposed model's ability was confirmed with a considerably low (RMSEP = 0.821) and (RSEP = 1.38).

The analysis of the residuals, which are defined as the difference between the experimental and the predicted data, revealed that the actual data was fitted satisfactorily in the proposed model. The normal probability of residuals plot (Fig. 5) evaluates the normality assumption. The points in the normal probability plot formed a straight line, which indicates that all the errors are nearly distributed [19]. The non-significant lack of fit term (0.39) implies the quadratic model's validity and there is no systematic variation [41].

Fig. 6 shows the predicted values versus the experimental values for %RE. As was shown, the close values of predicted and experimental data demonstrated the hypothesised model's predictability [42].

A Pareto chart helps to indicate the importance of the variable effect. It is a special form of bar graph, which exhibits the percentage effect of each term on the response. According to following equation:

$$P_i = \frac{\left(b_i\right)^2}{\sum b_i^2} \times 100 \tag{8}$$

Table 4
ANOVA for fit of regeneration efficiency (RE %)

Source of variation	Sum of Squares	Degree of freedom	Mean square	F-value	Prob > F	
Model	2792.53	9	310.28	127.87	< 0.0001	Significant
A	849.76	1	849.76	350.19	< 0.0001	
B	136.25	1	136.25	56.15	< 0.0001	
C	839.75	1	839.75	346.07	< 0.0001	
AB	24.50	1	24.50	10.10	0.0099	
AC	24.50	1	24.50	10.10	0.0099	
BC	40.50	1	40.50	16.69	0.0022	
A^2	487.66	1	487.66	200.97	< 0.0001	
B^2	28.15	1	28.15	11.60	0.0067	
C^2	283.58	1	283.58	116.87	< 0.0001	
Residual	24.27	10	2.43			
Lake of fit	6.77	5	1.35	0.39		Not significant
Pure error	17.50	5	3.50			
Core total	2816.80	19				

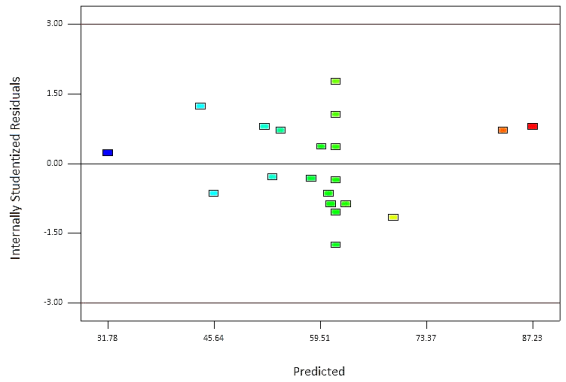

Fig. 5. The plot of normal probability of residuals.

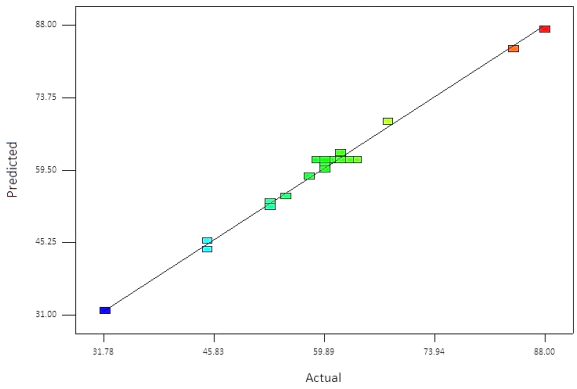

Fig. 6. Parity plot of actual and model predicted values of response variable.

Fig. 7 presents the effective variables and their interactions, arranged based on their relative importance. In this regard, Pareto Analysis revealed that current density and pH are the most significant parameters in RE [43].

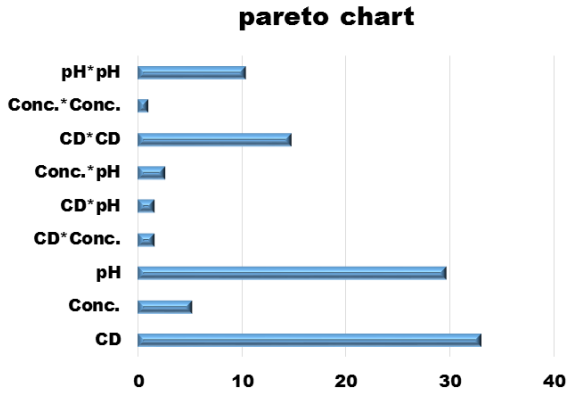

Fig. 7. Pareto graphic analysis.

3.4. Interactive effect of current density and pH

The interactive effect of current density and pH on %RE under the predetermined conditions is shown in Fig. 8. The maximum %RE was obtained at the current density of 0.18 A·cm^2 and at a pH of 2.35. Current density is one of the most important parameters affecting %RE as the %latter increases with the increase in the former. This observation is attributed to the production of active species oxidants, such as chlorine and OH, being promoted at a higher current density. The above mentioned powerful oxidants would attack and, thus, degrade organic molecules, which in turn increase %RE. The EC generation of OH on the anode surface (anodic oxidation) is as follows [32]:

$$H_2O \rightarrow OH^{\bullet} + H^+ + e^- \quad (9)$$

On the other hand, indirect oxidation of chloride ions caused the production of active chlorine, as illustrated in Eqs. (10)–(13) [32]:

$$Cl^- \leftrightharpoons Cl_{ads} + e^- \quad (10)$$

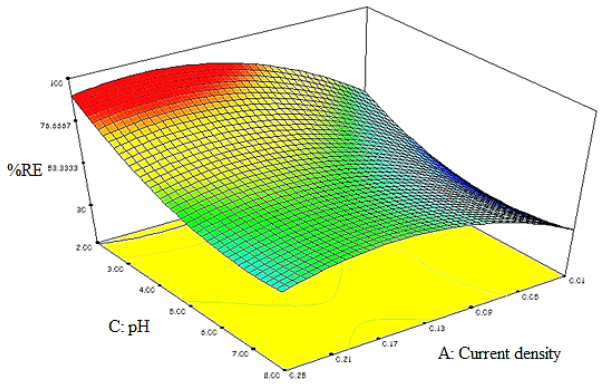

Fig. 8. 3D surface plot for the %RE of GAC as a function of current density and pH.

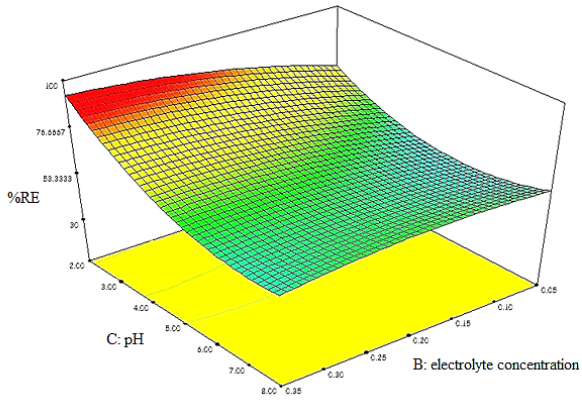

Fig. 9. 3D surface plot for the %RE of GAC as a function of electrolyte concentration and pH.

$$Cl^- + Cl_{ads} \leftrightharpoons Cl_2 + e^- \quad (11)$$

$$Cl_2 + H_2O \leftrightharpoons HOCl + H^+ + Cl^- \quad (12)$$

$$HOCl \leftrightharpoons OCl^- + H^+ \quad (13)$$

An individual experiment was carried out in acidic media in the absence of current. In this condition, below 10% RE indicates the slight desorption of the pollutant, due to the lack of oxidant species.

3.5. Interactive effect of electrolyte concentration and pH

Fig. 9 represents a three-dimensional response surface plot as a function of electrolyte concentration and pH at constant current density. Considering the interaction between the two main influential parameters, the maximum %RE of GAC was attained at the electrolyte concentration of 0.25 mol·L^{-1} and at a pH of 2.35. A low pH value (2–3) benefits EC regeneration of GAC since both anodic oxidation and indirect oxidation of chloride ions imply better performance in an acidic pH. In the NaCl solution, dependent on the electrolyte pH, two main oxidants, including hypochlorous acid and hypochlorite ion, were formed by molecular chlorine, as previously described in Eqs. (10)–(13). It should be noted that the production of hypochlorous acid, as a more powerful oxidant, is promoted in an acidic pH [32]. Furthermore, an increasing variation of %RE is observed with an increasing NaCl concentration. This is due to the fact that, at a high NaCl concentration, active chlorine generation was promoted, thus degradation of the dye is facilitated and, predictably, the %RE increased. Moreover, from an economic viewpoint, with the increase in NaCl concentration, the cell conductivity and subsequent current density increases at the same voltage; hence, energy consumption and the cost of the process would be noticeably decreased.

3.6. Energy consumption in optimal conditions

The amount of energy consumption in the EC regeneration process for 4 g of GAC is calculated by the following equation [26]:

Table 5
Energy consumption and current efficiencies of designed experiments at different operating condition

Experimental run	Energy consumption (kW·h·kg^{-1})	Current efficiency (%)	Regeneration efficiency (%)
1	0.68	16.95	45
2	1.48	9.21	53
3	1.48	10.95	63
4	2.28	6.21	55
5	1.48	10.78	62
6	1.48	10.61	61
7	0.68	19.97	53
8	2.28	9.49	84
9	1.48	15.30	88
10	2.28	6.78	60
11	2.85	5.24	58
12	1.48	11.13	64
13	0.68	16.95	45
14	1.48	10.43	60
15	0.11	72.35	32
16	1.48	10.78	62
17	2.28	7.68	68
18	1.48	10.48	60
19	0.68	22.61	60
20	1.48	10.26	59

$$W = \frac{VIt}{m} \quad (14)$$

where W is the energy consumption for GAC regeneration (kW·h·kg^{-1}), V the applied voltage (kV), I the current, t the time of the process (h) and m the mass of GAC (kg). Energy consumption and the current efficiencies of the designed experiments under different operating conditions are presented in Table 5. In this work, the energy consumption was calculated as 1.5 kW·h·kg^{-1}, which is lower than in

Table 6
A comparison of energy consumption of published articles with present study in optimal condition

Researcher	Electrolyte	Current density (A/cm^2)	Cathode	Anode	Energy consumption ($kW{\cdot}h{\cdot}kg^{-1}$)	RE%
Zhou [32]	NaCl	0.006	stainless steel	β-PbO_2	2.78	90
Weng [26]	NaCl	0.008	graphite	graphite	0.6492	91.1
Narbaitz [30]	NaCl	0.002	platinum	platinum	1.8	20
Present study	NaCl	0.18	graphite	Ti/Co-MnO_2	1.5	88

similar research, and proved that the proposed regeneration method is an economically feasible technique. A comparison of the energy consumption in published articles with the present study in optimal conditions is presented in Table 6.

3.7. Regeneration cycles

Reusing GAC for a second adsorption cycle, under optimum conditions, would be possible in a wastewater treatment process. However, a decreasing RE trend was observed with an increasing reuse time, which is attributed to incomplete recovery that, in turn, decreased the adsorption ability of GAC. After three sequential adsorption–regeneration cycles, only 23% declination was observed in %RE, which confirmed the reuse feasibility of the regenerated GAC (Fig. 10). The slight decrease in the micro pore volume during the regeneration process would be the main reason for this descendant trend [32].

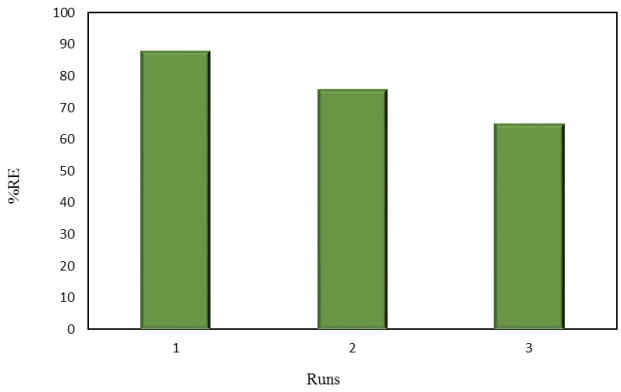

Fig. 10. Regeneration efficiency percentage during three times regeneration.

3.8. GAC analysis

The BET (Brunauer–Emmett–Teller) results indicated that the surface area decreased from 840.04 to 605.57 $m^2{\cdot}g^{-1}$ during the saturation process. The determination of specific areas of meso pores and micro pores was performed using the BET test. Based on the results, the significantly decreasing surface area of micro pores in saturated GAC demonstrated that the adsorption of AR18 has occurred in the micro pores. The surface area of the regenerated GAC was 784.78 $m^2{\cdot}g^{-1}$. The %RE calculated through the investigation of the surface area of fresh, saturated and regenerated GAC, using Eq. (3), achieved around 77.28%. Moreover, a scanning electron microscope (SEM) was employed to conduct photomicrography of the GACs (fresh and regenerated). Based on the SEM results, fresh GAC, as shown in Fig. 11, has an irregular shape and an identical porous surface. The image (Fig. 11) illustrates that the porous structure of the GAC has not changed remarkably after the EC treatment process in optimum conditions.

3.9. Electrode analysis

3.9.1. SEM Observation

The SEM (JSM/840A) was utilised to investigate the electrodes' morphology before and after Co-MnO_2 coating, as depicted in Figs. 12a and b. As the images show, the surface coverage in the modified electrode increased, which led to an increase in the active sites on the electrode surface. The modified electrode's stability is one of the important factors in EC oxidation examined by using SEM before (Fig. 12b) and after (Fig. 12c) EC regeneration of GAC for 20 h. The SEM images were observed and compared to investigate the changes in the electrode's surface during the process. In this regard, the small amount of change on the electrode's surface after 20 h of EC regeneration confirms the modified electrode's stability [44].

3.9.2. Cyclic voltammetry

Fig. 13 depicts the cyclic voltammetry of the anode performed at 50 mV s^{-1} in 1 M H_2SO_4 at room temperature. Whereas, the typical value expected for O_2 evolution in an acidic solution is 1.02 V vs. Ag/AgCl [45], the onset potential of Ti/Co-MnO_2 as an anode electrode is 1.87 V vs. Ag/AgCl. The higher potential value for the modified electrode indicates that oxygen evolution was kinetically suppressed. As is shown in Fig. 13a, the Ti electrode has the onset potential of 1.5 V vs. Ag/AgCl for O_2 evolution. In contrast, the onset potential value measured for the modified electrode (Fig. 13b) is 0.37 V higher than the base electrode. The insignificant difference between the onset potential of the modified electrode before (Fig. 13b) and after tests (Fig. 13c) confirms that the modified electrode's quality has not changed noticeably during the EC regeneration process. It is worth mentioning, since O_2 evolution is a side reaction in anodic oxidation of pollutants, that the higher onset potential for O_2 evolution and, therefore, higher current efficiency for pollutant oxidation is desired [44].

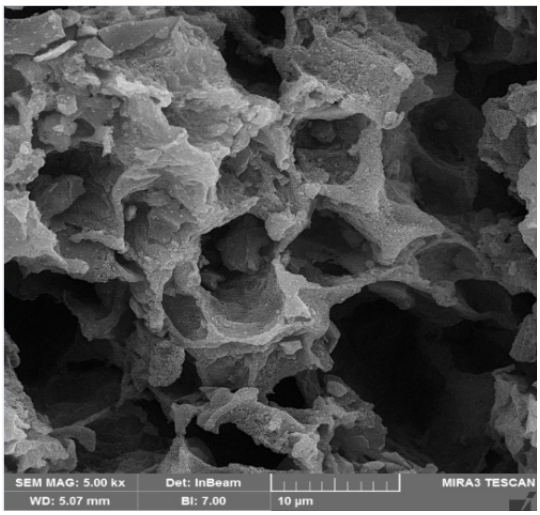

(a)

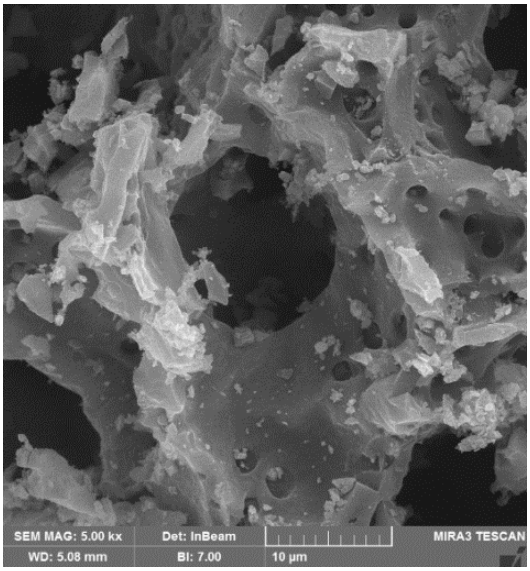

(b)

Fig. 11. SEM image of (a) Fresh and (b) Regenerated granular activated carbon.

3.10. Feasibility of industrial scale

Although thermal regeneration of GAC is known as an industrial method, this technique's drawbacks, such as high energy consumption, attrition and carbon loss, have restricted its application in future projects. In this regard, many researchers and industries have investigated the possibility of employing other regeneration methods on a large scale. Among these methods, EC regeneration, due to environmental compatibility, safety, selectivity, no addition of chemicals and low temperature, does have the potential to be employed on a large scale. Moreover, electrode materials significantly influence the performance and economics of EC regeneration. Taking this into consideration, the modified electrode has

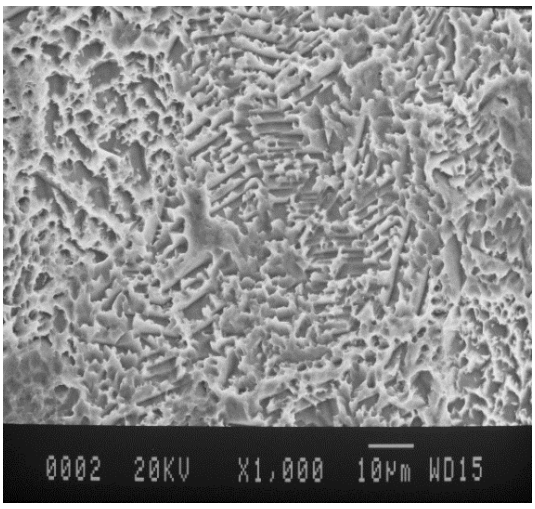

(a)

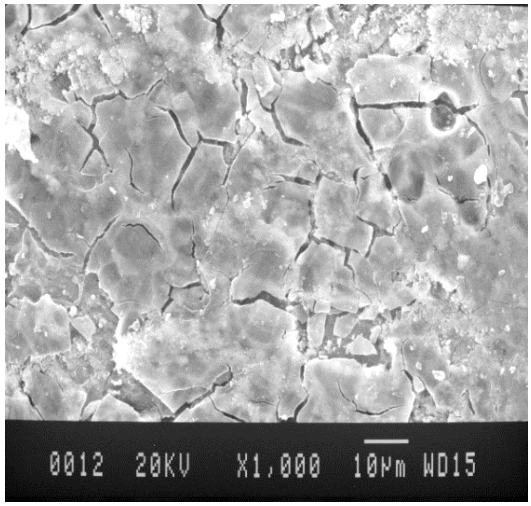

(b)

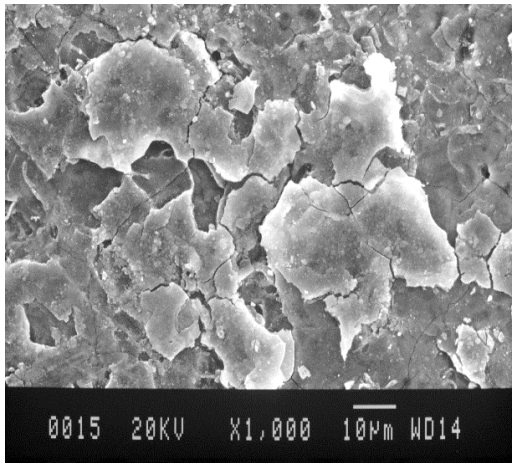

(c)

Fig. 12. The SEM image of (a) Ti electrode without coating, (b) Ti/Co–MnO_2 electrode fresh and (c) Ti/Co–MnO_2 after 20 h of electrochemical regeneration.

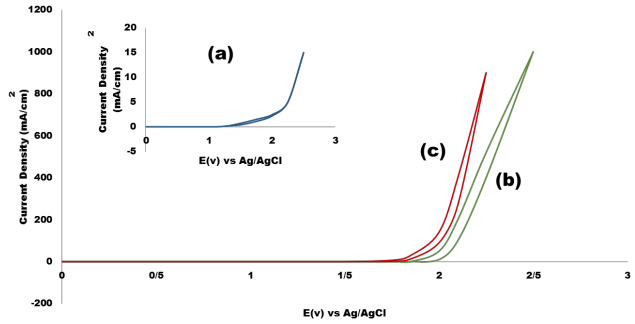

Fig. 13. Comparison of cyclic voltammograms obtained on different electrode after reaching steady state: (a) Ti net, (b) Ti/Co-MnO_2 and (c) used modified electrode.

been proposed in this study. As previously mentioned, low energy consumption and reuse feasibility has confirmed the economic potential of the suggested method in industrial applications.

4. Conclusion

EC regeneration of the exhausted GAC on novel non-active anodes of modified Co-MnO_2 is the most economical and environmentally acceptable option. The electrode material significantly affects the performance of the EC regeneration. The modified electrode used in this project led to more generation of active species and, hence, higher efficiency. The EC degradation of AR18 should be attributed to both the anodic oxidation and the indirect oxidation of chloride. The regeneration parameters, such as current density, electrolyte concentration and pH, were investigated to optimise performance and to improve the cost-effectiveness of the process. The optimisation of the process was conducted using RSM based on CCD. The optimised condition for maximum RE was at a current density of 0.18 ($A{\cdot}cm^{-2}$), an electrolyte concentration of 0.25 ($mol{\cdot}L^{-1}$) and a pH of 2.35. Under these conditions the highest %RE was 88%. Based on the attained empirical model, current density is the most influential parameter. Verification of the proposed model's computing determination coefficient ($R^2 = 0.9914$) indicated a good agreement between the quadratic model and the experimental results. In addition, the energy consumption calculation in EC regeneration of saturated GAC under optimum conditions revealed that the proposed method would be a promising technique in regeneration processes.

Acknowledgment

The authors are grateful to the University of Bu-Ali Sina for financial support of this research.

References

[1] Y. Bulut, N. Gözübenli, H. Aydın, Equilibrium and kinetics studies for adsorption of direct blue 71 from aqueous solution by wheat shells, J. Hazard. Mater., 144(1–2) (2007) 300–306.
[2] Z. Ai, J. Li, L. Zhang, S. Lee, Rapid decolorization of azo dyes in aqueous solution by an ultrasound-assisted electrocatalytic oxidation process, Ultrason. Sonochem., 17(2) (2010) 370–375.
[3] Z. Berizi, S.Y. Hashemi, M. Hadi, A. Azari, A.H. Mahvi, The study of non-linear kinetics and adsorption isotherm models for Acid Red 18 from aqueous solutions by magnetite nanoparticles and magnetite nanoparticles modified by sodium alginate, Water Sci. Technol., 74(5) (2016) 1235–1242.
[4] M.J. Iqbal, M.N. Ashiq, Adsorption of dyes from aqueous solutions on activated charcoal, J. Hazard. Mater., 139(1) (2007) 57–66.
[5] M.T. Yagub, T.K. Sen, S. Afroze, H.M. Ang, Dye and its removal from aqueous solution by adsorption: a review, Adv. Colloid Interf., 209 (2014) 172–184.
[6] M.O. Omorogie, J.O. Babalola, E.I. Unuabonah, Regeneration strategies for spent solid matrices used in adsorption of organic pollutants from surface water: a critical review, Desal. Water Treat., 57(2) (2016) 518–544.
[7] F.K. Yuen, B. Hameed, Recent developments in the preparation and regeneration of activated carbons by microwaves, Adv. Colloid Interf., 149(1–2) (2009) 19–27.
[8] R. Berenguer, J. Marco-Lozar, C. Quijada, D. Cazorla-Amorós, E. Morallon, Electrochemical regeneration and porosity recovery of phenol-saturated granular activated carbon in an alkaline medium, Carbon, 48(10) (2010) 2734–2745.
[9] M.-W. Jung, K.-H. Ahn, Y. Lee, K.-P. Kim, J.-S. Rhee, J.T. Park, K.-J. Paeng, Adsorption characteristics of phenol and chlorophenols on granular activated carbons (GAC), Microchem. J., 70(2) (2001) 123–131.
[10] N. Brown, E. Roberts, A. Garforth, R. Dryfe, Electrochemical regeneration of a carbon-based adsorbent loaded with crystal violet dye, Electrochim. Acta, 49(20) (2004) 3269–3281.
[11] G. Zhang, S. Wang, Z. Liu, Ultrasonic regeneration of granular activated carbon, Environ. Eng. Sci., 20(1) (2003) 57–64.
[12] S.-R. Ha, S. Vinitnantharat, H. Ozaki, Bioregeneration by mixed microorganisms of granular activated carbon loaded with a mixture of phenols, Biotechnol. Lett., 22(13) (2000) 1093–1096.
[13] P.M. Coss, C.Y. Cha, Microwave regeneration of activated carbon used for removal of solvents from vented air, JAPCA J. Air Waste Manage., 50(4) (2000) 529–535.
[14] A. Bagreev, H. Rahman, T.J. Bandosz, Thermal regeneration of a spent activated carbon previously used as hydrogen sulfide adsorbent, Carbon, 39(9) (2001) 1319–1326.
[15] O. Belyaeva, N. Golubeva, T. Krasnova, A. Yakusheva, Developing a technology for the regeneration of active coal after pyridine adsorption from wastewater, Chem. Sustain. Dev., 17 (2009) 243–247.
[16] R.M. Narbaitz, J. Cen, Electrochemical regeneration of granular activated carbon, Water Res., 28(8) (1994) 1771–1778.
[17] S.-J. Park, S.-D. Yeo, Supercritical extraction of phenols from organically modified smectite, Sep. Sci. Technol., 34(1) (1999) 101–113.
[18] L.C. Toledo, A.C.B. Silva, R. Augusti, R.M. Lago, Application of Fenton's reagent to regenerate activated carbon saturated with organochloro compounds, Chemosphere, 50(8) (2003) 1049–1054.
[19] J.B. Parsa, F. Jafari, Sono-Fenton regeneration of granular activated carbon saturated with Rhodamine B: Optimization using response surface methodology, Chem. Eng. Commun., 204(9) (2017) 1070–1081.
[20] R. Berenguer, J. Marco-Lozar, C. Quijada, D. Cazorla-Amorós, E. Morallón, Comparison among chemical, thermal, and electrochemical regeneration of phenol-saturated activated carbon, Energ. Fuel, 24(6) (2010) 3366–3372.
[21] L. Wang, N. Balasubramanian, Electrochemical regeneration of granular activated carbon saturated with organic compounds, Chem. Eng. J., 155(3) (2009) 763–768.
[22] Y.-D. Dai, C. Yuan, C. Huang, P.-C. Chiang, Regeneration of spent carbon nanotubes by electrochemical oxidation over RuO_2/Ti electrode, Sep. Purif. Technol., 178 (2017) 207–214.
[23] R. Narbaitz, A. Karimi-Jashni, Electrochemical regeneration of granular activated carbons loaded with phenol and natural organic matter, Environ. Technol., 30(1) (2009) 27–36.

[24] N. Brown, E. Roberts, A. Chasiotis, T. Cherdron, N. Sanghrajka, Atrazine removal using adsorption and electrochemical regeneration, Water Res., 38(13) (2004) 3067–3074.
[25] R. Narbaitz, J. Cen, Alternative methods for determining the percentage regeneration of activated carbon, Water Res., 31(10) (1997) 2532–2542.
[26] C.-H. Weng, M.-C. Hsu, Regeneration of granular activated carbon by an electrochemical process, Sep. Purif. Technol., 64(2) (2008) 227–236.
[27] M. Zhou, Q. Dai, L. Lei, C.a. Ma, D. Wang, Long life modified lead dioxide anode for organic wastewater treatment: electrochemical characteristics and degradation mechanism, Environ. Sci. Technol., 39(1) (2005) 363–370.
[28] K. Jardak, A. Dirany, P. Drogui, M.A. El Khakani, Electrochemical degradation of ethylene glycol in antifreeze liquids using boron doped diamond anode, Sep. Purif. Technol., 168 (2016) 215–222.
[29] H. Zhang, L. Ye, H. Zhong, Regeneration of phenol-saturated activated carbon in an electrochemical reactor, J. Chem. Technol. Biot.: International Research in Process, Environmental & Clean Technology, 77(11) (2002) 1246–1250.
[30] R.M. Narbaitz, J. McEwen, Electrochemical regeneration of field spent GAC from two water treatment plants, Water Res., 46(15) (2012) 4852–4860.
[31] J.B. Parsa, F. Jafari, Electrochemical regeneration of granular activated carbon saturated with Rhodamine B in a fluidized electrochemical reactor, Desal. Water Treat., 94 (2017) 174–180.
[32] M. Zhou, L. Lei, Electrochemical regeneration of activated carbon loaded with p-nitrophenol in a fluidized electrochemical reactor, Electrochim. Acta, 51(21) (2006) 4489–4496.
[33] O. Zanella, D. Bilibio, W.L. Priamo, I.C. Tessaro, L.A. Féris, Electrochemical regeneration of phenol-saturated activated carbon–proposal of a reactor, Environ. Technol., 38(5) (2017) 549–557.
[34] A. Azizi, M.R. Alavi Moghaddam, R. Maknoon, E. Kowsari, Investigation of enhanced Fenton process (EFP) in color and COD removal of wastewater containing Acid Red 18 by response surface methodology: evaluation of EFP as post treatment, Desal. Water Treat., 57(30) (2016) 14083–14092.
[35] L. Wang, Z. Chen, H. Wen, Z. Cai, C. He, Z. Wang, W. Yan, Microwave assisted modification of activated carbons by organic acid ammoniums activation for enhanced adsorption of acid red 18, Powder Technol., 323 (2018) 230–237.
[36] O. De Nora, A. Nidola, P.M. Spaziante, Manganese dioxide electrodes, Google Patents, 1978.
[37] K.P. Singh, S. Gupta, A.K. Singh, S. Sinha, Experimental design and response surface modeling for optimization of Rhodamine B removal from water by magnetic nanocomposite, Chem. Eng. J., 165(1) (2010) 151–160.
[38] J.B. Parsa, M. Abbasi, Modeling and optimizing of sonochemical degradation of Basic Blue 41 via response surface methodology, Cent. Eur. J. Chem., 8(5) (2010) 1069–1077.
[39] B.K. Körbahti, A. Tanyolaç, Electrochemical treatment of simulated textile wastewater with industrial components and Levafix Blue CA reactive dye: Optimization through response surface methodology, J. Hazard. Mater., 151(2–3) (2008) 422–431.
[40] K.P. Singh, N. Basant, A. Malik, G. Jain, Modeling the performance of "up-flow anaerobic sludge blanket" reactor based wastewater treatment plant using linear and nonlinear approaches—a case study, Anal. chim. Acta, 658(1) (2010) 1–11.
[41] R. Meng, X. Yu, Investigation of ultrasound assisted regeneration of Ni–bentonite with response surface methodology (RSM), Appl. Clay Sci., 54(1) (2011) 112–117.
[42] B. Hameed, I. Tan, A. Ahmad, Optimization of basic dye removal by oil palm fibre-based activated carbon using response surface methodology, J. Hazard. Mater., 158(2–3) (2008) 324–332.
[43] F.N. Chianeh, J.B. Parsa, Electrochemical degradation of metronidazole from aqueous solutions using stainless steel anode coated with SnO_2 nanoparticles: experimental design, J. Taiwan Inst. Chem. Eng., 59 (2016) 424–432.
[44] J.B. Parsa, Z. Merati, M. Abbasi, Modeling and optimizing of electrochemical oxidation of CI Reactive Orange 7 on the Ti/Sb–SnO_2 as anode via Response Surface Methodology, J. Indust. Eng. Chem., 19(4) (2013) 1350–1355.
[45] X. Chen, F. Gao, G. Chen, Comparison of Ti/BDD and Ti/SnO_2–Sb_2O_5 electrodes for pollutant oxidation, J. Appl. Electrochem., 35(2) (2005) 185–191.